Heat treatment and failure risk of large automotive plastic molds: a fracture mechanics approach and property assessment

D. Firrao, P. Matteis, G. Scavino, G. Ubertalli, M. G. Ienco, A. Parodi, M. R. Pinasco, E. Stagno, R. Gerosa, B. Rivolta, G. Silva, A. Silvestri, A. Ghidini

Molds for plastic automotive components such as bumpers and dashboards are usually machined from large pre-hardened steel blocks. Due to the dimension of the blooms, the heat treatment produces mixed microstructures, continuously varying with the distance from the quenched surface, at which fracture toughnesses lower than those appropriate for a fully quenched and tempered metallurgical condition are usually associated. Furthermore, final fabrication machining exposes, in part of the mold's surface, the steel that was at heart during both ingot casting and bloom heat treatment. The response of the mold to defects (for example, microcracks from weld bed deposition) or events (for example, incomplete formed plastic object extraction) that can conceivably cause failure during service (and in a few cases actually did), depends on the steel properties, that in turn depend upon the heat treatment and the microstructure. A pointwise survey of the mechanical properties of some commercial blooms, actually used to machine bumper molds, has shown usual and expected values of hardness and of tensile properties, but, indeed, a low range of fracture toughness, suggesting that the latter is a critical characteristic of this steel and that fracture mechanics verifications, already usual in other fields of industry, should dutifully be applied to the molds' design. The relationship between the mechanical properties, the morphology of the fracture surfaces and the microstructure has been also investigated.

Keywords: plastic mold steel, metallography, mechanical properties, fracture toughness, fractography

INTRODUCTION

Large forged steel blooms (typically 1x1 m in section and more than 1 m in length) are used to fabricate plastic molds, in turn employed to form automotive components, such as bumpers and dashboards, made of thermoplastics, usually polypropylene or reinforced ABS.
The stress pattern applied to the molds in service arises from the polymer's injection pressure and from the thermal gradients, and could be enhanced by notch effects and by defects of various origin (particularly weld bed depositions effected without the heat treatment that could be recommended for smaller components). Stresses may be significantly raised by abnormal operations, e.g. incomplete extraction of already formed objects.
Each mold is expected to produce a few millions of pieces in its life, corresponding to the production run of one car model, thus fatigue effects should also be considered. Wear induced by the reinforced resins flow may be severe and may be an additional cause for crack nucleation, with the flowing resin infiltrating cracks and acting as a wedge.
For economic and logistic reasons, the traditional production cycle (rough machining, heat treating and finishing) has been abandoned and commonly substituted by machining pre-hardened blooms.
The most commonly used steel grade is 1.2738 (or 40CrMnNiMo8-6-4, ISO 4957 standard (1)), a heat-treatable, 0.4% C, high-hardenability, low-alloy steel (Table 1).
The section of the bloom is usually comparable to the section of the original ingot (because larger ingots are not feasible); thus a sensible reduction ratio is usually obtained by repeated forging steps, each consisting of alternated elongation and compression cycles. The total deformation is much less than that obtained in rolling and not comparable in the effects, because each step achieves only a limited reduction ratio (1.5 is a possible value).
Depending on the size, dehydrogenization can take a few days, whereas the durations of the austenitizing and tempering stages can be 1 to 2 days. Usually, blooms are austenitized in the 840÷880 °C temperature range, then quenched in oil and tempered in the 550÷600 °C temperature range (more than one tempering stage may be applied) to obtain a final 330÷300 HB hardness. Heating stages are usually executed in air.
Since forging yields a rough shape with deep decarburations occurring during heating, external material removal (usually performed in a commercial warehouse) may be up to 20 mm (plus scale). Furthermore, blooms may be sawn to requested size (often asymmetrically); blooms for bumper molds are usually sawn to yield a U shape.
The dimension of the blooms exceeds the very high harde-

D. Firrao, P. Matteis, G. Scavino, G. Ubertalli
Dip. di Sc. dei Materiali ed Ing. Chimica - Politecnico di Torino

M. G. Ienco, A. Parodi, M. R. Pinasco, E. Stagno
DCCI - Università di Genova

R. Gerosa, B. Rivolta, G. Silva, A. Silvestri
Dip. Meccanica – Politecnico di Milano

A. Ghidini
Lucchini Sidermeccanica S.p.A.

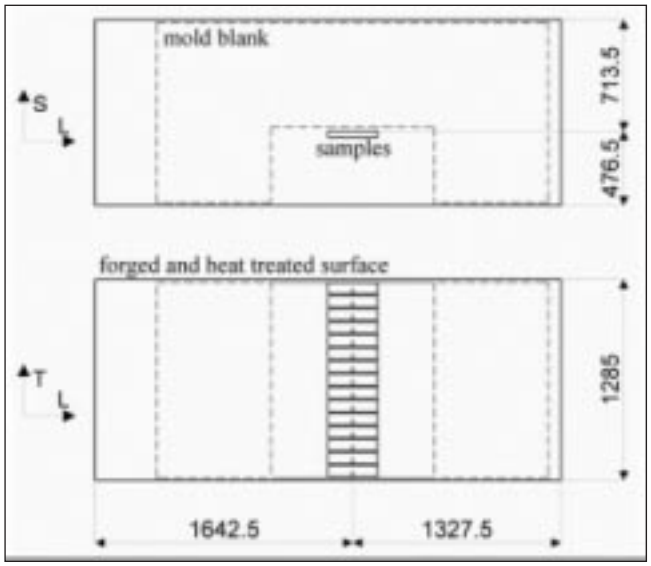

Fig. 1 – 38 mm thick fracture toughness samples cut at increasing depths inside bloom C.

Fig. 1 – Campioni di tenacità a frattura, spessi 38 mm, ricavati a profondità crescenti entro il blumo C.

nability of steel 1.2738 (2 - 3), thus in large oil-quenched blooms different microstructures occur at increasing depths, all of them being affected by the subsequent tempering.
The final mold shape is obtained in the mold-machining shop by chip-removal and/or electrical-discharge machining, followed by grinding with or without polishing in selected areas and by local surface treatments; upon request, shape corrections are performed also by welding additions.
Due to the sawing and machining operations, any of the microstructures occurring at different positions in the original bloom can be found at the mold face, where notch effects and welding thermal defects are often present. Previous studies have assessed the deleterious influence of the mixed microstructures, due to a slack quench, upon the toughness of quenched and tempered low alloy steels (4 - 5); nevertheless, whereas the fracture toughness of other tool steels was already studied (6 - 7 - 8), the same property has not yet been extensively analyzed in the present mold steels, nor even in any tool steel piece of the above reported size.
Thus, the relevant steel properties, particularly fracture toughness, fatigue and wear resistance, should be studied as a function of the microstructure as well as of the position in respect to the quenched surfaces.

SAMPLING

Three original blooms, namely A, B and C, were fabricated in the form of parallelepipeds used for manufacturing bumper molds. Bloom A was used for the initial trial runs (9). Bloom C had the following original dimensions (resulting from forging): 2970 (L) x 1285 (T) x 1190 (S) mm. The original dimensions of bloom B were estimated as being 2240 (L) x 900 (T) x 900 (S) mm.
The L direction defines the long ingot casting and forging axis, whereas the S and T directions are thought not to be influenced by the casting and forging procedures and are defined only as a conventional reference system.
The results of the average chemical analysis of bloom B and of the heat chemical analysis of bloom C are reported in Table 1.
Series of thick (38 mm) fracture toughness specimens were obtained from bloom C (Fig. 1), whereas smaller specimens were obtained from both blooms in analogous positions and used for metallography, tension and hardness testing. Charpy V-notched specimens were obtained from the broken halves of two of the fractured toughness specimens.
The depth of a point is generally defined as its distance from the nearest blank surface (i.e., forged and heat treated); nevertheless in presenting results for series of specimens cut in successive positions from a bloom surface to the opposite one, through its center, reference to the first surface will be kept for consistency. Due to the large size of fracture toughness specimens, their depth is calculated as that of the fracture initiation zone.

METALLOGRAPHY

Due to the larger original size, bloom C microstructures are presented first.

	C	Cr	Mn	Ni	Mo	Si	S	P
Grade 1.2738 - 40CrMnNiMo8-6-4	0.35 - 0.45	1.8 - 2.1	1.3 - 1.6	0.9 - 1.2	0.15 - 0.25	0.2 - 0.4	<0.03	<0.03
Bloom B	0.39	2.1	1.5	1.0	0.20	0.23	0.010	0.011
Bloom C	0.42	2.0	1.5	1.1	0.21	0.37	0.002	0.006

Table 1 – Compositional limits for the plastic mold steel grade 1.2738 and results of the average chemical analysis of bloom B and of the heat chemical analysis of bloom C.

Tabella 1 – Forcelle di composizione dell'acciaio per stampi per materie plastiche 1.2738 e risultati dell'analisi chimica media del blumo B e dell'analisi chimica di colata del blumo C.

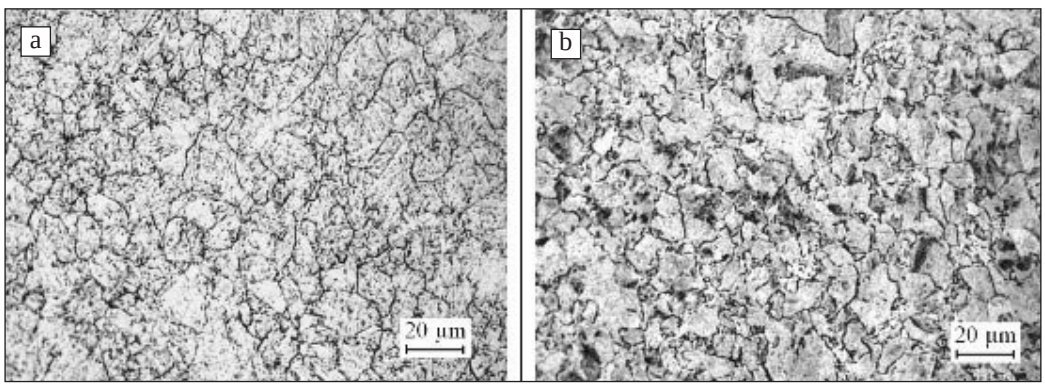

Fig. 2 – Previous austenitic grain boundaries close to the surface (a) and to the core (b) of bloom C. Bechet-Beaujard etch. Austenitic grain size, measured by the intercept method, was ~10.5 and ~9 µm, respectively.

Fig. 2 – Precedenti bordi di grano austenitici vicino alla superficie (a) ed al cuore (b) del blumo C. Attacco Bechet-Beaujard. La dimensione del grano austenitico, misurata con il metodo delle intercette, era circa pari a 10,5 ed a 9 µm, rispettivamente.

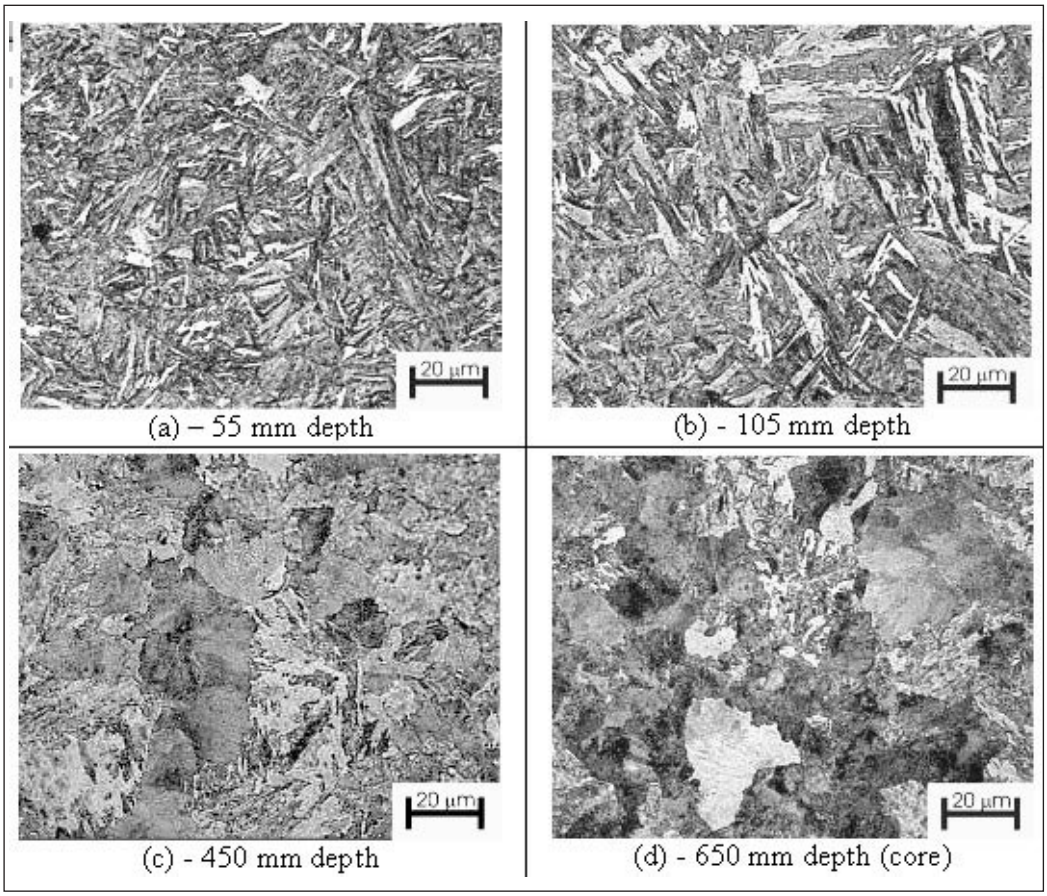

Fig. 3 – Metallographic constituents at increasing depths in bloom C; Nital etch. (a) 55 mm depth, tempered martensite, residual austenite transformed during tempering. (b) 105 mm depth, lower bainite modified by tempering, residual austenite transformed during tempering. (c) 450 mm depth, fine and ultra-fine pearlite, upper bainite modified by tempering. (d) 650 mm depth (core), fine pearlite, upper bainite modified by tempering (showing coarser carbides).

Fig. 3 – Costituenti metallografici a profondità crescente nel blumo C; attacco Nital. (a) profondità 55 mm, martensite rinvenuta, austenite residua trasformata durante il rinvenimento. (b) profondità 105 mm, bainite inferiore modificata dal rinvenimento, austenite residua trasformata durante il rinvenimento. (c) profondità 450 mm, perlite fine ed ultra-fine, bainite superiore modificata dal rinvenimento. (d) profondità 650 mm (cuore), perlite fine, bainite superiore modificata dal rinvenimento (caratterizzata da carburi ingrossati).

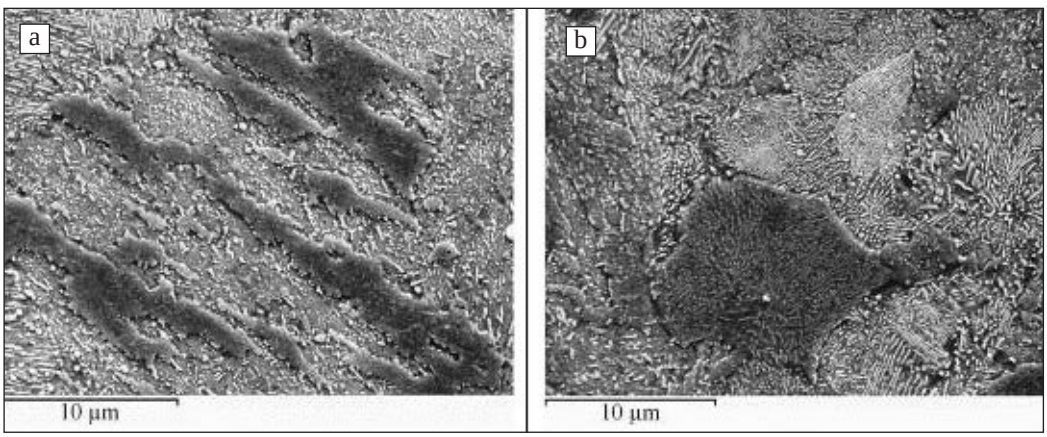

Fig. 4 – SEM details of metallographic constituents at 650 mm depth (core) in bloom C: upper bainite modified by tempering (a) and fine pearlite (b). Nital etch.

Fig. 4 – Microscopia elettronica a scansione. Dettagli dei costituenti metallografici a profondità di 650 mm (cuore) nel blumo C: bainite superiore modificata dal rinvenimento (a) e perlite fine (b). Attacco Nital.

Bloom C

The microstructure of bloom C was examined at 9 representative positions, by using standard Nital etch, at increasing depth from surface to core, along a segment in T direction; observed surfaces were perpendicular to L direction. Furthermore, the austenitic grain size was measured in two position, close to the core and to the surface, respectively, by using the Bechet-Beaujard etch (Fig. 2, (10)). The linear intercept procedure yielded ~9 and ~10.5 µm, slightly smaller at core.

Although no observations were made upon the as-quenched bloom, as-quenched microstructures had nevertheless to be hypothesized in order to explain the observed tempered ones.

Lower cooling speeds at increasing depth during quenching produce different metallographic constituent, in particular, going from surface to core, martensite, residual austenite, lower and upper bainite, ultra-fine and fine pearlite were found.

At the lowest depths (Fig. 3a, b) the actual microstructure of bloom C is mainly acicular, so that orientation relationships can be approximately traced first from austenite grains to martensite and lower bainite laths formed during quenching and then from martensite laths to still aligned carbides precipitated during tempering. Nevertheless, some isolated bright area punctuated by small dark carbides can be traced back to austenite that was retained after quenching and then transformed during the tempering stages. Comparison between Fig. 3a and Fig. 3b shows that the microstructure slightly coarsens at increasing depths, while tempered martensite laths are increasingly substituted by lower bainite packets, the latter probably affected by carbide coarsening during the tempering stages.

At intermediate depths, ultra-fine and then fine pearlite (formed directly during the quenching stage) gradually appears alongside the previously described constituents. No pearlite is found at 285 mm depth; some rare, ultra-fine pearlite can be detected at 370 mm depth and finally a significant fraction of ultra-fine and fine pearlite is observed at 450 mm depth (Fig. 3c). Also at these intermediate depths, lower bai-

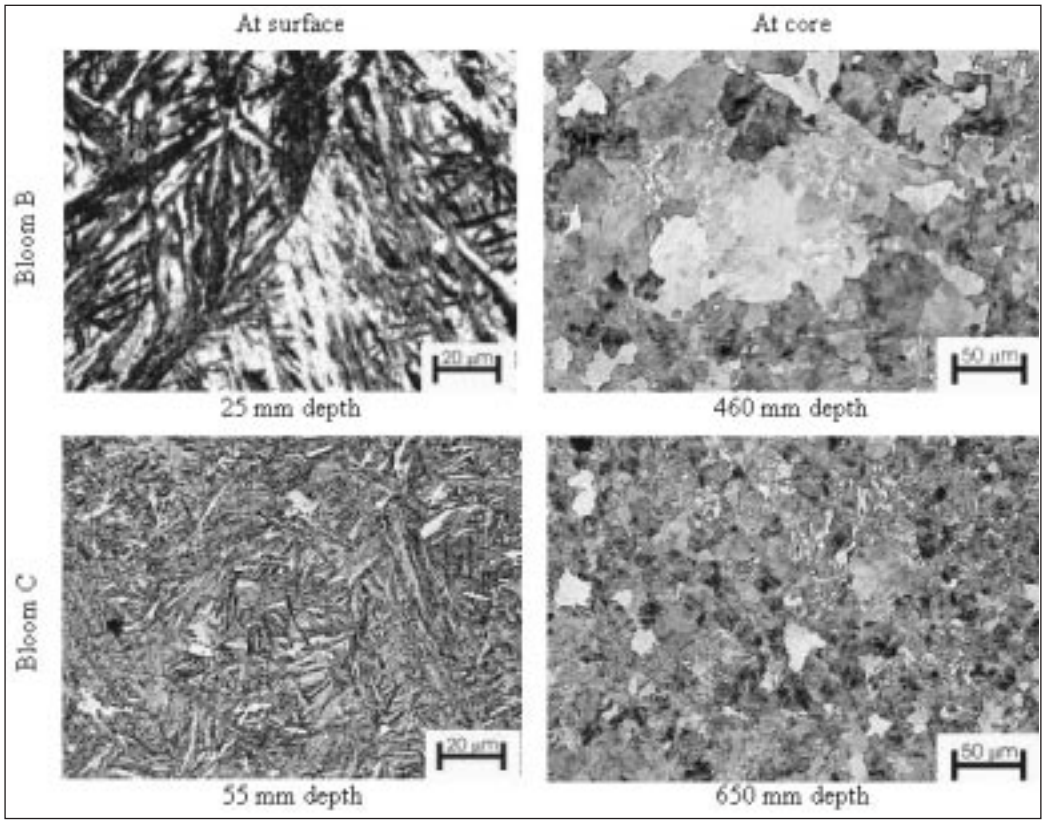

Fig. 5 – Comparison of the microstructures of blooms B (core at 450 mm depth) and C (core at 642 mm depth); Nital etch. The microstructure of the former is coarser, probably due to coarser previous austenitic grains, both near the surface and at heart.

Fig. 5 – Confronto tra le microstrutture dei blumi B (cuore a profondità di 450 mm) e C (cuore a profondità di 642 mm); attacco Nital. La microstruttura del primo è più grossolana, probabilmente a causa del precedente grano austenitico più grossolano, sia vicino alla superficie, sia al cuore.

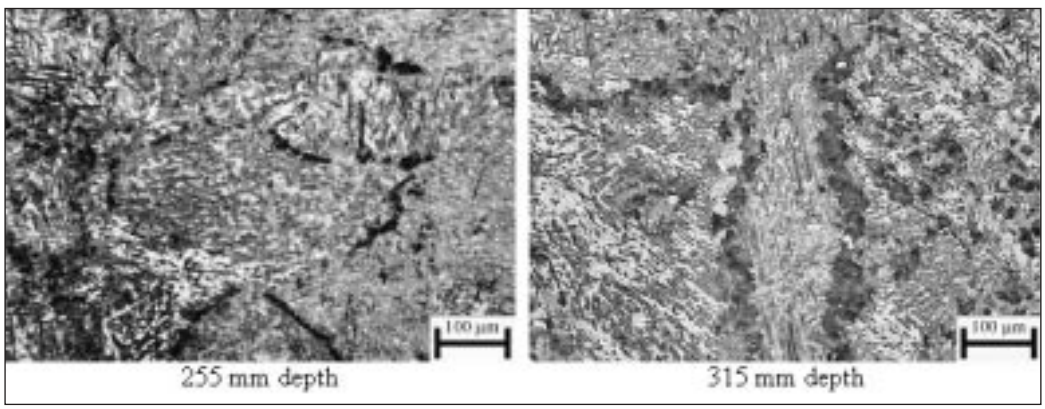

Fig. 6 – Microstructural evolution at intermediate depths in bloom B. Pearlite appears starting from previous austenite grain boundaries. Nital etch.

Fig. 6 – Evoluzione microstrutturale a profondità intermedie nel blumo B. La perlite comincia ad apparire lungo i precedenti bordi di grano austenitici. Attacco Nital.

nite is gradually replaced by upper bainite, the latter being once more affected by carbide coarsening during the tempering stages.
Close to the bloom heart (Fig. 3d), fine pearlite is the main constituent, together with some bainitic area. Scanning electron microscopy (SEM) shows fine details of both constituents (Fig. 4).

Bloom B

The microstructures were examined at 14 representative depths (some of them in different laboratories); it showed the same sequence of metallographic constituents from surface to core, although with some segregations (not observed in bloom C).
The comparisons of the microstructure of the two blooms (Fig. 5) in two positions, respectively near to surface and close to core, showed that bloom B had a much coarser microstructure, due to a larger previous austenitic grain size.
Furthermore, in bloom B, at intermediate depth, pearlite occurred at supposed previous austenite grain boundaries (Fig. 6); the same phenomenon was not so evident in bloom C.
Finally, whereas in bloom C a significant fraction of bainite is still detected at core, in bloom B the microstructure in the same position is almost fully pearlitic.

MECHANICAL TESTING

Hardness and tensile tests

Hardness and tensile tests were performed upon specimens obtained at increasing depths. The tensile specimens were oriented in the L direction and the hardness was measured upon surfaces perpendicular to the S directions.

Bloom C. The hardness versus depth curve pertaining to bloom C, that was obtained by HV_{100} tests at 9 positions (each average of 5 indentations), monotonically decreases from surface to core (Fig. 7) and shows values in the 316-363 HV range. A relationship between hardness and as-quenched microstructure may be hypothesized as follows. The initial decrease, from 360 HV at surface to about 330 HV at 200 mm depth, may be related to the transition from tempered martensite to tempered bainite; the hardness plateau of about 330 HV between 200 and 540 mm depth grossly corresponds to the mainly bainitic microstructures; finally, the minimum value at core (316 HV) is clearly related to the presence of pearlite.

Bloom B. The hardness profile (Fig. 7) was determined by HRC test measures (each average of nine or more indenta-

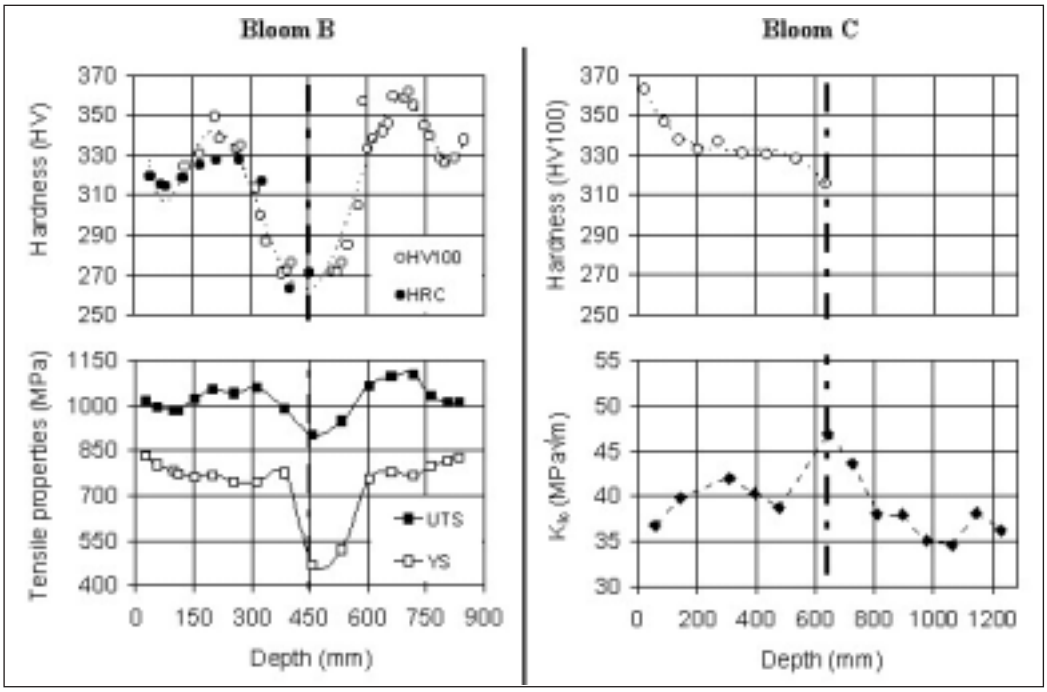

Fig. 7 – Hardness, ultimate tensile strength (UTS) and yield stress (YS) in respect to depth in bloom B; hardness and fracture toughness in respect to depth in bloom C. Hardness test surfaces perpendicular to direction S; uniaxial tensile tests with orientation L and fracture toughness tests with orientation LT.

Fig. 7 – Durezza, tensione di rottura (UTS) e tensione di snervamento (YS) in funzione della profondità nel blumo B; durezza e tenacità a frattura in funzione della profondità nel blumo C. Prove di durezza su superfici perpendicolari alla direzione S; prove di trazione uniassiali con orientamento L e di tenacità a frattura con orientamento LT.

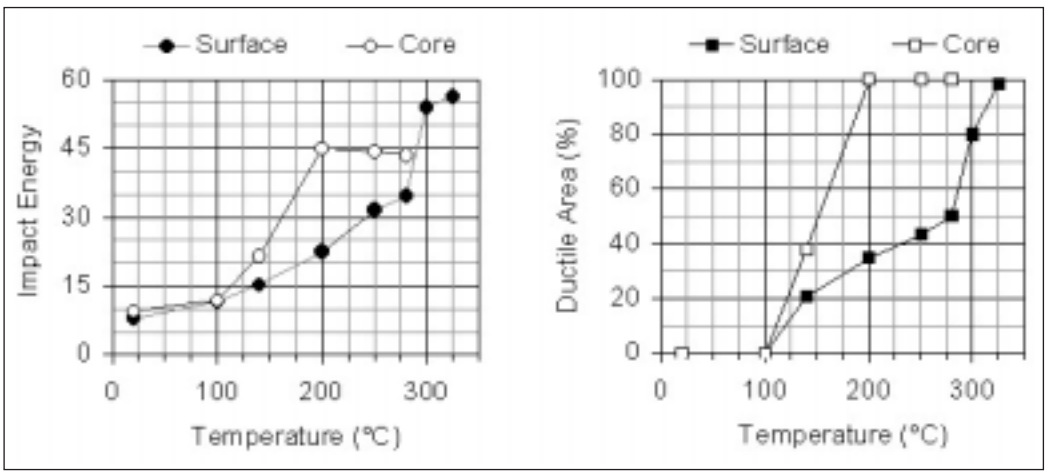

Fig. 8 - Ductile-to-brittle transition curves at surface and at core of bloom C, obtained from V-notched Charpy specimens tested at increasing temperatures. Impact energy and fracture appearance vs. test temperature. LT sample orientation.

Fig. 8 - Curve di transizione duttile - fragile alla superficie ed al cuore del blumo C, ottenute da campioni Charpy con intaglio a V rotti a temperature crescenti. Resilienze e percentuale duttile della superficie di frattura in funzione della temperatura di prova. Orientamento dei campioni: LT.

tions, then converted to HV, at 10 positions) and HV_{100} test measures (at 32 positions). It shows values comprised in the 263÷362 HV range. The curve is almost symmetrical respect to the bloom's centerline and presents a sharp decrease at the center, but also shallow maxima at an intermediate depth of about 200 mm.
Curves of ultimate tensile strength and of yield stress vs. depth were determined by 18 uniaxial tensile tests upon cylindrical specimens (~ 7 mm diameter). The diagram of the ultimate tensile strength as a function of depth is similar to the corresponding hardness curve, showing a sharp decrease at core and shallow maxima at about 250 mm depth; the yield stress presents first a continuos decrease with depth, and then a sharp minimum at core.
Reasons for the shape of the hardness and the ultimate tensile stress curves at intermediate depths in bloom B are not evident, nevertheless it may be attributed to different actual tempering durations. The minima of hardness and of tensile properties at core are due to the same reason as the corresponding hardness minimum in bloom C.

Comparison of hardness Properties. The hardness at core is significantly higher in bloom C than in bloom B (316 vs. 263 HV), despite the smaller size of the latter bloom, a fact that may be attributed to a finer previous austenitic grain size and to a larger fraction of not-pearlitic constituents in the former one.
Notwithstanding some similarity of the hardness profile at the center of the blooms, bloom C is overall more homogeneous in hardness than bloom B.

Fracture toughness and impact tests (Bloom C)

Fracture toughness tests were performed upon the samples cut from bloom C with LT orientation (according to ASTM E399 and E1820). Generally, a pop-in occurred before the maximum. The specimen thickness, that was selected to allow for much larger expected K_{Ic} values, is abundant in respect to the validation limit and the curves of force versus crack opening displacement do not show any significant plastic contribution (not linear).
K_{Ic} values present a limited variation from surface to core of bloom C (Fig. 7), with a trend to slightly higher toughnesses at core. Typical values are about 36 MPa√ m close to surface and 47 MPa√ m close to core.
Charpy-V impact tests were performed at increasing temperatures, from 20 °C to 325 °C, by using two series of 8 and of 6 samples, cut from bloom C positions close to the surface or to the core, respectively. The resulting transition curves (Fig. 8) show brittle-to-ductile transition temperatures of

about 270 °C close to the surface and about 150 °C close to the core, based on fracture appearance (50% FATT). Impact energies at room temperature are about 10 J.

FRACTOGRAPHY

The prior austenite grains control all the fracture surfaces of the K_{Ic} test samples, as observed by SEM. Intergranular brittle fractures alternate with cleavage ruptures at the lowest distances from the fracture surface. Intergranular fractures become increasingly less brittle as the distance increases, showing ductile dimples on the grain boundaries.
The 60 mm depth K_{Ic} sample fracture surface appears generally brittle with almost no ductile dimples being detected, except in the lateral shear lips (which are less than 0.25 mm wide) and in small transition zones between adjacent brittle domains. The fracture initiation zone does not show significant signs of blunting.
Brittle surface features are either grain facets, due to intergranular rupture (Fig. 9a), or cleavage facets (Fig. 9b, c). Adjacent grain facets are identified by observing the overall morphology and particularly the evident grain corners, while isolated grain facets, bounded by surfaces due to other fracture mechanisms (either cleavage facets or small ductile transition zones), can be recognized by comparing their local morphology (Fig. 9d). Fig. 9e seems to indicate brittle fracture through a local segregation. It is thus hypothesized that the fracture path follows the grain boundaries found in a convenient position and orientation in respect to the overall fracture plane, with some cuts through the grains by cleavage. Small ductile transition zones are generally found between cleavage regions of different orientation (pertaining to different grains) and between cleavage and intergranular regions. The occurrence of intergranular fracture should be related to elemental segregations at grain boundaries, probably due to the long heat treatment durations (11).
The relevant boundaries should be those of the previous austenite grains. The sizes of the intergranular fracture facets and of the uninterrupted cleavage regions, being in reasonable agreement with the above-mentioned austenitic grain size measurements, confirm such a hypothesis.
The fracture surface of the 230 mm depth K_{Ic} sample (Fig. 10) also shows a prevalent (somehow decreased) fraction of cleavage areas (Fig. 10a), but only rare evidences of brittle intergranular fracture (Fig. 10b, c). On the contrary, it shows a significant fraction of areas of ductile fracture with shallow largely hemispherical dimples about 1 μm wide (Fig. 10d, e). These dimples were clearly different in morphology in respect to the smaller, but proportionally deeper, ones found in the ductile transition zones between adjacent grains (Fig. 10e); because they appear in a depth range corresponding to the transition from tempered martensite to lower bainite, it is hypothesized that they develop due to bainite carbides.
The fracture surface of the 395 mm depth K_{Ic} sample (Fig. 11) shows an increasing fraction of the above-mentioned shallow ductile fracture (detail), almost no evidence of intergranular fracture and a still large fraction of cleavage surfaces.
The fracture surface of the 565 mm depth K_{Ic} sample (Fig. 12) shows mainly cleavage and ductile areas similar to those of the specimens at lower depths, with an increasing trend for the ductile fraction; some isolated areas with evident transversal signs of intergranular fracture (Fig. 12b) and fractures through a pearlite colony (Fig. 12c) are also observed.
Finally, the fracture surface of the 645 mm depth (core) K_{Ic} sample (Fig. 13) again shows mixed cleavage and ductile areas, with the latter slightly increasing in fraction while moving away from the fracture initiation line.
Moreover, from the 560 mm and 140 mm depth K_{Ic} specimens (depth from opposite surface), two cross-section samples were extracted in the centre of the fracture surfaces and polished so that it was possible to observe the fracture contour. The samples were etched with the Bechet-Beaujard solution in order to observe the previous austenitic grain boundaries (Fig. 14). The previous austenitic grains are more heterogeneous and somehow larger in the 140 mm depth sample than in the 560 mm depth one. The fracture path seems to follow, at times, the prior austenitic grain boundaries.

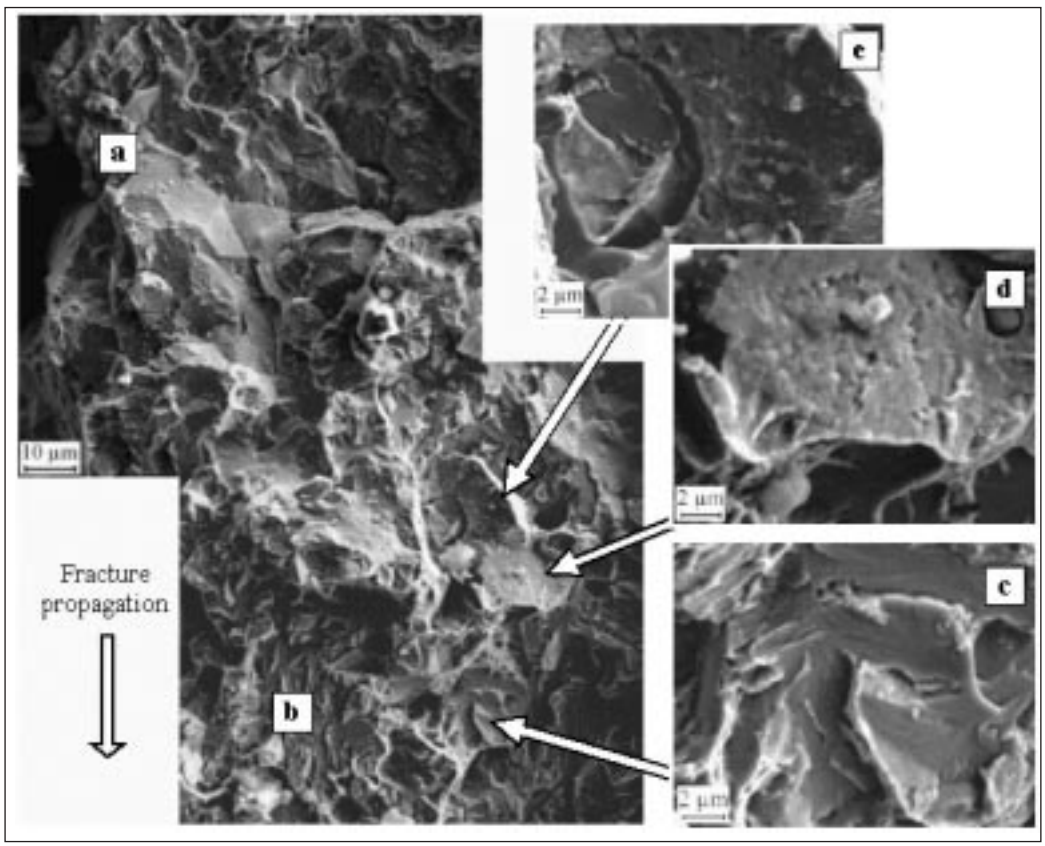

Fig. 9 – Fracture surface of 60 mm depth K_{Ic} sample. Adjacent intergranular (a) and cleavage (b) fracture areas. Details: cleavage zone (c), fracture through a segregated zone (d), isolated intergranular facets (d, e).

Fig. 9 – Superficie di frattura del campione di tenacità a frattura a profondità di 60 mm. Aree adiacenti di frattura intergranulare (a) e di clivaggio (b). Dettagli: zona di clivaggio (c), frattura attraverso una zona con segregazioni (d), facce intergranulari isolate (d, e).

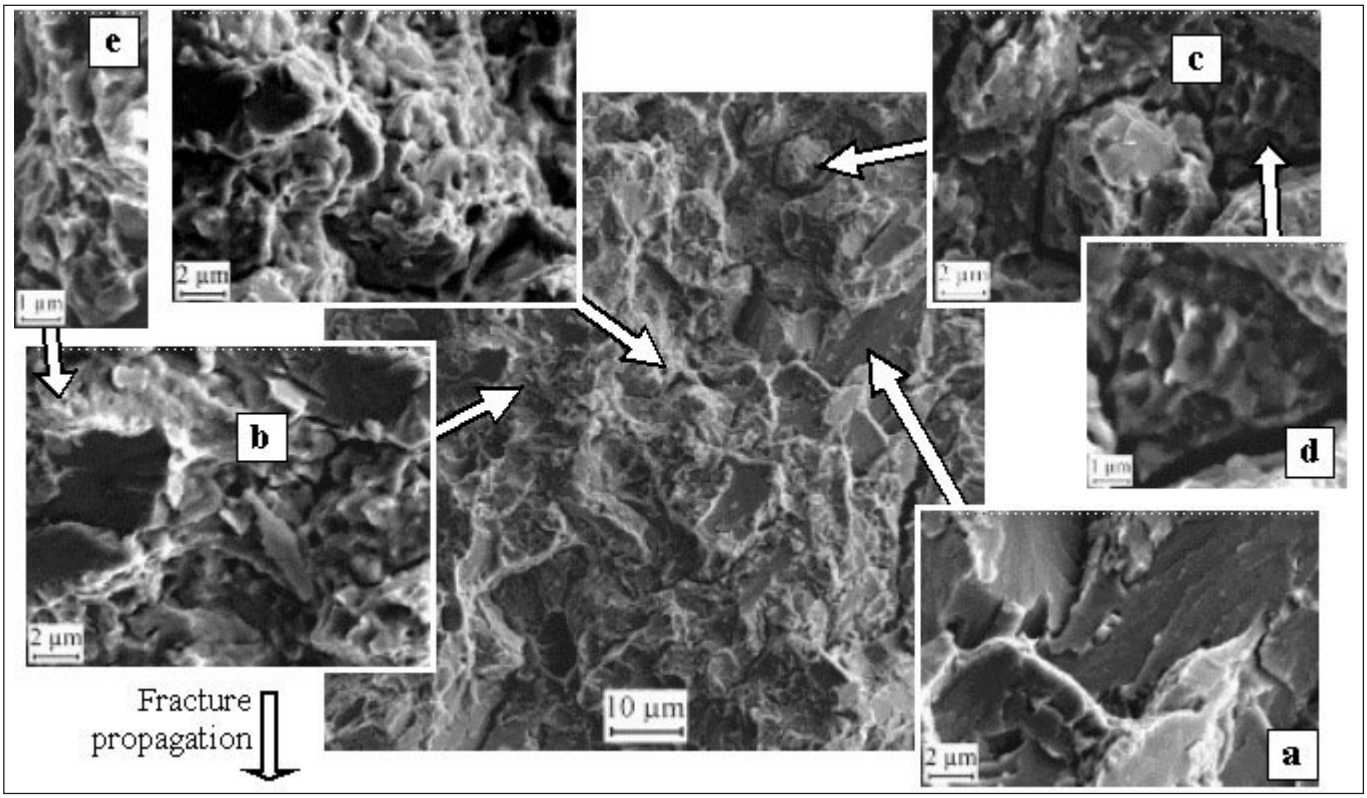

Fig. 10 – Fracture surface of 230 mm depth K_{Ic} sample. Decreasing (but yet large) fraction of cleavage areas (a) in respect to the 60 mm depth sample. Limited evidences of brittle intergranular failure: isolated portions of grain facets (b), secondary cracks (c). Areas of ductile fracture showing shallow, 1µm wide regular dimples (d), as opposed to the smaller but proportionally deeper irregular dimples found in ductile transition zones between adjacent grains (e).

Fig. 10 – Superficie di frattura del campione di K_{Ic} a profondità di 230 mm. Frazione decrescente (ma ancora rilevante) di area di clivaggio (a) rispetto al campione a profondità di 60 mm. Limitati fenomeni di frattura intergranulare: porzioni isolate di facce di grani (b), cricche secondarie (c). Aree di frattura duttile caratterizzate da microvuoti regolari, larghi circa 1 µm, poco profondi (d), se paragonati con i microvuoti irregolari, più piccoli ma proporzionalmente più profondi, osservati nelle zone duttili di transizione tra grani adiacenti (e).

Fig. 11 – Fracture surface of 395 mm depth K_{Ic} sample. Increasing fraction of dimpled fracture.

Fig. 11 – Superficie di frattura del campione di tenacità a frattura a profondità di 395 mm. Frazione crescente di frattura con microvuoti.

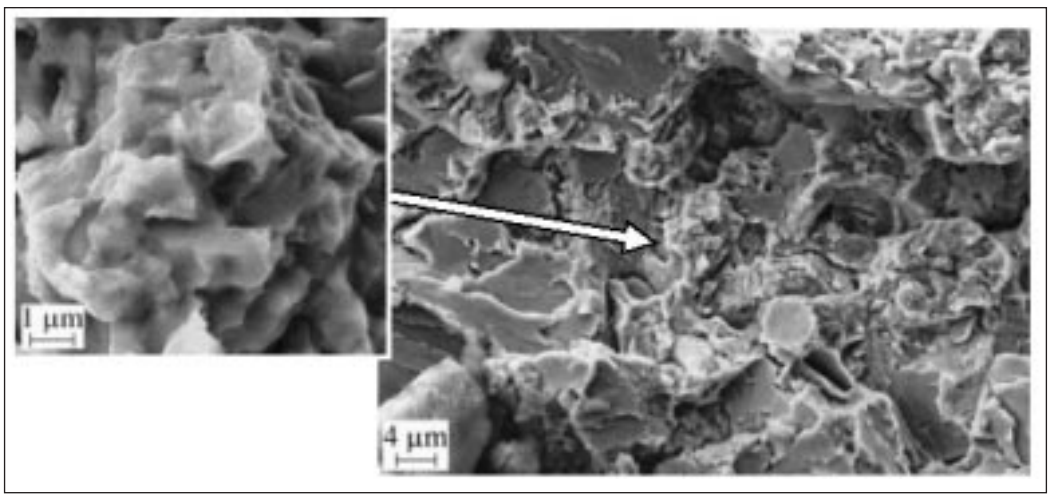

DISCUSSION AND CONCLUSIONS

Mixed microstructures occur throughout the blooms. Tempered martensite occurs only close to the surface and steeply decreases with depth; upper and lower bainites (modified by tempering) are the overall prevalent constituents; pearlite gradually appears at increasing depth and becomes the main constituent at core. Nevertheless, blooms obtained from different steelmaking practices may show remarkable differences in the austenitic grain size and in the presence of local segregation, presumably due to different forging and heat treating schedules.

The hardness and the tensile properties exibit significant variations inside the blooms, but, except a small region at core, are in overall compliance with the usually specified values.

The fracture toughness values are exceptionally low for a quenched and tempered steel, considering the achieved strength. Previous measures upon steel 1.2738 samples that were individually quenched and tempered resulted in values of fracture toughness in excess of 100 MPa√ m (albeit not fully valid), even at somewhat higher strength levels (9); thus, the observed low toughness must be attributed to the slack quench, in turn due to the large dimensions of the blooms used to fabricate molds.

Coherently with the low fracture toughness, the plain-strain fracture prevalently occurs by decohesion either along grain boundaries or along cleavage planes, meaning that the ductile-to-brittle transition barrier is not overcome; ductile areas

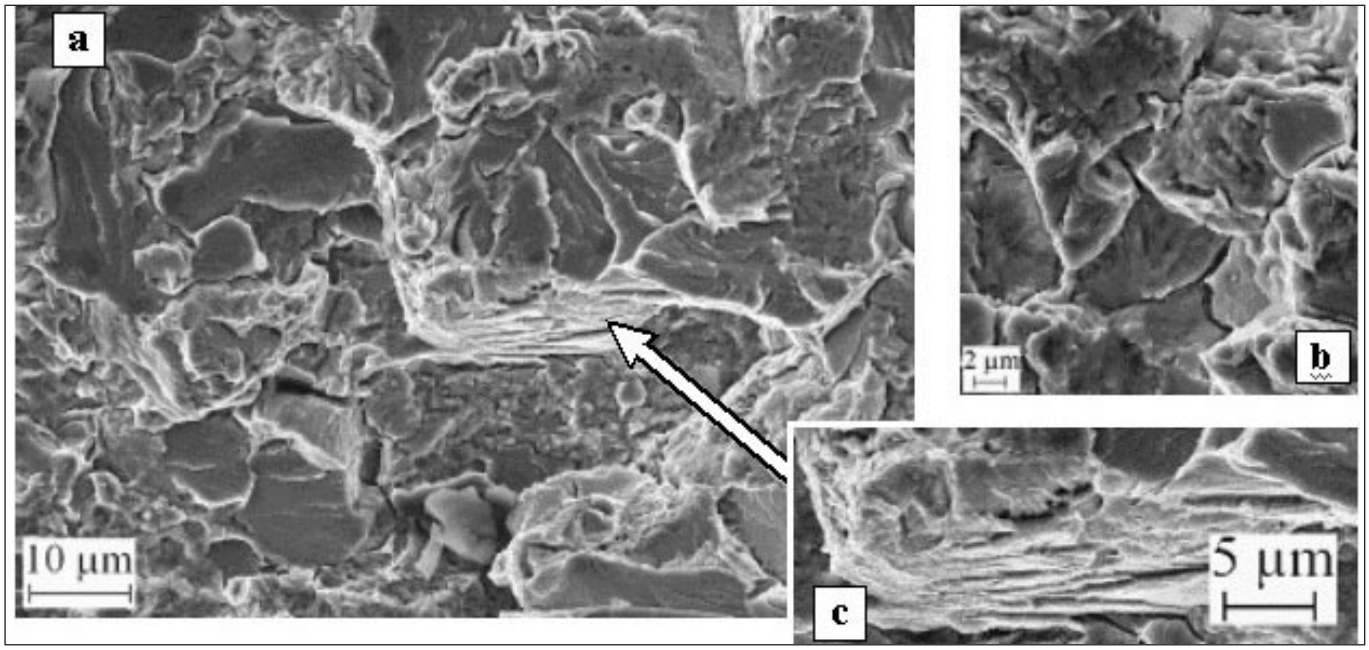

Fig. 12 – Fracture surface of 565 mm depth (core) K_{Ic} sample. Cleavage and dimpled areas, as seen at smaller depths, with increasing ductile fraction, in the majority of the fracture surface (a); some isolated areas of intergranular failure (b); isolated pearlite colony fractures (c).

Fig. 12 – Superficie di frattura del campione di tenacità a frattura a profondità di 565 mm (cuore). Aree con microvuoti ed aree di clivaggio, come alle profondità inferiori, con frazione duttile crescente, nella maggior parte della superficie di frattura (a); qualche area isolata di frattura intergranulare (b); isolate fratture di colonie perlitiche (c).

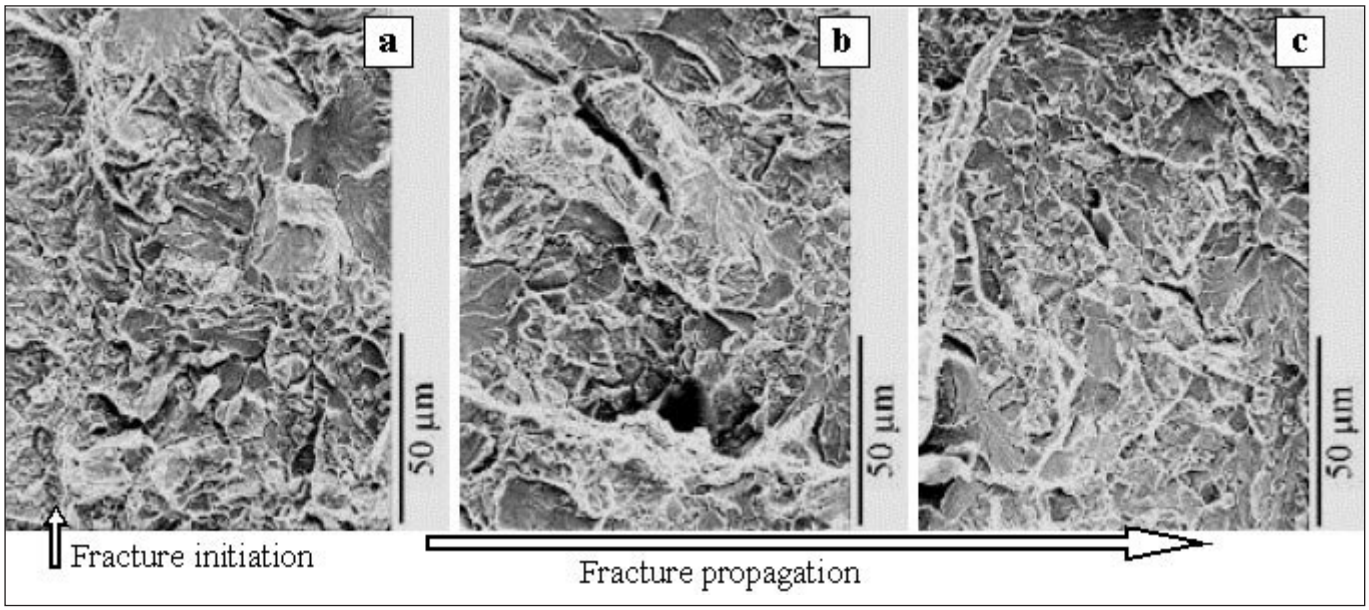

Fig. 13 – Fracture surface of 645 mm depth K_{Ic} sample. Fracture initiation at the pre-crack tip (a) and fracture propagation at 0.2 and 0.4 mm distance (b, c) from the same tip. Mixed cleavage and ductile areas.

Fig. 13 – Superficie di frattura del campione di tenacità a frattura a profondità di 645 mm. Inizio della frattura presso il vertice della precricca (a) e propagazione della frattura a 0,2 ed a 0,4 mm di distanza (b, c) dal medesimo vertice. Aree miste di clivaggio e di frattura duttile.

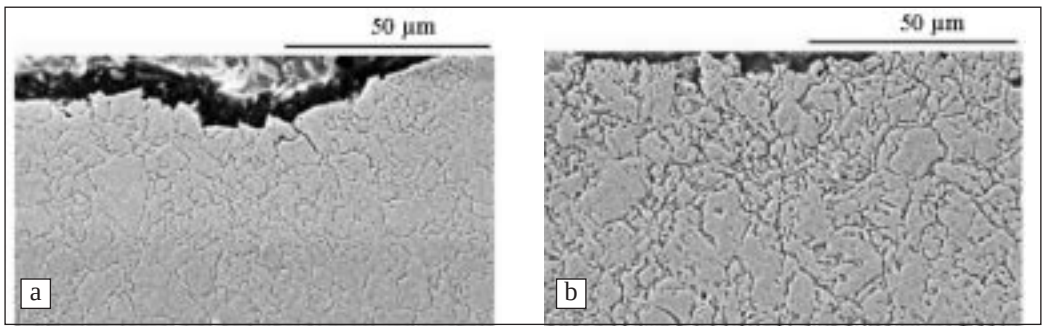

Fig. 14 - Prior austenitic grain close to the fracture surfaces of K_{Ic} specimens at 725 mm (a) and at 1145 mm (b) depth in bloom C (center at 642 mm depth, distances from opposite surface 560 mm (a) and 140 mm (b)).

Fig. 14 - Precedente grano austenitico presso le superfici di frattura dei campioni di tenacità a frattura a profondità di 725 mm (a) e 1145 mm (b) nel blumo C (centro a 642 mm, distanze dalla superficie opposta 560 mm (a) e 140 mm (b)).

with shallow dimples occur only in a limited fraction of the surface of the grain boundaries. The moderate fracture toughness increase at core can be attributed to energy consumption in these ductile regions, which are absent close to the surface and increase towards the center of the original bloom.
The low absorbed impact energy values and the high brittle-to-ductile transition temperatures are consistent with these results and show that, in consideration of the usual service temperatures of the plastic molds, this steel is generally used in the brittle range of its brittle-to-ductile transition curve.
In the practice of the plastic mold industries, the fracture toughness is neither measured, nor used for verification; nevertheless, based on the present work, this property appears critical for the steels used to fabricate the larger molds. Actually, reported brittle in-service mold failures could be related to the above-mentioned low fracture toughness. Thus, the use of fracture mechanics verification methods should be recommended during the molds design, as long as such low toughness steel is used.

ACKNOWLEDGEMENTS

L. Vitrano, H.C.M. Stampi SpA, for steel procurement.
Italian Ministry for Education, University and Research, for financial support by research grant PRIN 2003091205.
Maurizio Chiarbonello and Roberto Spadotto, for experimental work performed during their master of science thesis and graduate thesis, respectively.

REFERENCES

1. UNI EN ISO 4957:2002, Acciai per utensili (UNSIDER).
2. D. FIRRAO, P. MATTEIS, G. SCAVINO, G. UBERTALLI, M.G. IENCO, A.PARODI, P. PICCARDO, M.R. PINASCO, E. STAGNO, R. GEROSA, B. RIVOLTA, G. SILVA, Proc. 30th Convegno Nazionale AIM. Vicenza, Italy (2004). Paper No. 50, p. 1-11.
3. ASTM A255/99, Standard test method for determining hardenability of steels.
4. G. SACHS, G.S. SANGDAHL, W.F. BROWN, Iron Age, Nov. 23, p 59-63 and Nov. 30, p 76-80, 1950.
5. X.Z. ZHANG, J.F. KNOTT, Acta Mater., Vol. 47, No. 12, p 3483-3495, 1999.
6. A. BAUS, J.C. CHARBONNIER, H.P. LIEURADE, B. MARANDET, L. ROESCH, G. SANZ, Rev. Met, 72, p 891-935, 1975.
7. E. MOSCA, R. PARTENGO, R. ZOCCHI, Met. It., 67, 1975, p 562-567.
8. O. E. OKORAFOR, Mat. Sci. Tecn., 1987, vol. 3, p 118-124.
9. D. FIRRAO, P. MATTEIS, M. VASSALLO, Proc. 11th Int. Conf. on Fracture. Turin, Italy (2005). Paper No. 5590, p. 1-6.
10. S. BECHET, L. BEAUJARD, Rev. Met. 52, p 830-836, 1955.
11. C.L. BRIANT, S.K. BANERJI, Int. Met. Reviews, No. 4, p 164-199, 1978.

ABSTRACT

TRATTAMENTO TERMICO E RISCHIO DI FRATTURA DI GRANDI STAMPI PER MATERIE PLASTICHE PER USO AUTOMOBILISTICO: APPROCCIO MEDIANTE LA MECCANICA DELLA FRATTURA E DETERMINAZIONE DELLE RELATIVE PROPRIETÀ.

Parole chiave: acciaio, tratt. termici, mecc. frattura, microscopia elettronica, prove meccaniche, selezione materiali

Gli stampi per particolari in materia plastica usati nell'industria automobilistica, come per esempio paraurti e cruscotti, sono solitamente lavorati per asportazione di truciolo da grandi blocchi di acciaio prebonificato. L'asportazione di materiale nel corso della lavorazione espone, in parte della superficie dello stampo, l'acciaio che era a cuore durante i processi di colata e di trattamento termico. La risposta dello stampo a difetti (per esempio, microcricche originate da apporti di saldatura) oppure incidenti (per esempio, estrazione incompleta del pezzo formato), i quali possono causare rotture in servizio (in qualche caso ciò è realmente avvenuto), dipende dalle proprietà dell'acciaio, che a loro volta dipendono dal trattamento termico e dalla microstruttura. Pertanto, è stata svolta un'indagine puntuale delle microstrutture e delle proprietà meccaniche di alcuni blumi commerciali (Tabella 1), effettivamente usati per produrre stampi per paraurti.
A causa delle elevate dimensioni dei blumi, il trattamento termico produce microstrutture miste, variabili con continuità in funzione della distanza dalla superficie temprata. In prossimità della superficie si osserva prevalentemente martensite rinvenuta, la cui frazione, tuttavia, decresce rapidamente con la profondità; le bainiti, superiore ed inferiore (modificate dal rinvenimento), sono i costituenti prevalenti nell'insieme; infine, la perlite appare gradualmente a profondità più elevate e diventa il principale costituente a cuore (Fig. 3). Blumi ottenuti mediante diverse pratiche industriali possono presentare notevoli differenze riguardo alla dimensione del grano austenitico (Fig. 5) ed alla presenza di segregazioni (Fig. 6).
Sono stati riscontrati valori usuali ed attesi di durezza e di proprietà a trazione (ad eccezione di una piccola regione a cuore), ma valori di tenacità a frattura eccezionalmente ridotti (nonostante un lieve incremento a cuore, Fig. 7), dell'ordine di 40 MPa√ m, inferiori a quelli propri di una condizione metallurgica di tempra completa e rinvenimento (considerando il livello di resistenza a trazione ottenuto). Nel corso di precedenti misure, campioni del medesimo acciaio, temprati singolarmente e rinvenuti conseguendo livelli di resistenza a trazione alquanto superiori, hanno fornito tenacità dell'ordine di 100 MPa√ m; pertanto, la ridotta tenacità a frattura deve essere attribuita alla incompletezza dell'effetto di tempra, a sua volta causata dalle grandi dimensioni dei blumi e degli stampi.
Le ridotte resilienze riscontrate con prove Charpy a temperature ambiente e l'elevata temperatura di transizione fragile-duttile (Fig. 8) indicano che l'acciaio in esame viene normalmente impiegato a temperature comprese nella regione di comportamento fragile.
Nelle condizioni di deformazione piana a temperatura ambiente determinate dalle misure di K_{Ic}, la frattura avviene prevalentemente mediante decoesione in corrispondenza dei bordi dei grani oppure dei piani di clivaggio (Fig. 9), il che è una prova ulteriore che la barriera della transizione fragile-duttile non viene superata; si osservano aree duttili soltanto in una frazione limitata delle superfici di frattura (Fig. 10). Il moderato incremento della tenacità a frattura a cuore è attribuibile al consumo di energia in queste aree duttili, le quali sono assenti nei campioni più superficiali e costituiscono frazioni crescenti delle superfici di frattura all'aumentare della profondità dei campioni esaminati (Fig. 11, Fig. 12).
In conclusione, si ritiene che la tenacità a frattura sia una caratteristica critica per questi acciai e che le verifiche di tolleranza dei difetti con i metodi derivati dalle teorie di meccanica della frattura, ormai comuni in altri ambiti industriali, dovrebbero esser attentamente applicati al progetto degli stampi.